

# Mesoscopic simulations of anisotropic chemically-powered nanomotors

Pierre de Buyl\*

Instituut voor Theoretische Fysica, KU Leuven B-3001, Belgium

## Abstract

Chemically powered self-propelled colloids generate a motor force by converting locally a source of energy into directed motion, a process that has been explored both in experiments and in computational models. The use of active colloids as building blocks for nanotechnology opens the doors to interesting applications, provided we understand the behaviour of these elementary constituents. We build a consistent mesoscopic simulation model for self-propelled colloids of complex shape with the aim of resolving the coupling between their translational and rotational motion. Considering a passive L-shaped colloidal particle, we study its Brownian dynamics and locate its center of hydrodynamics, the tracking point at which translation and rotation decouple. The active L particle displays the same circling trajectories that have been found experimentally, a result which we compare with the Brownian dynamics model. We put forward the role of hydrodynamics by comparing our results with a fluid model in which the particles' velocities are reset randomly. There, the trajectories only display random orientations. We obtain these original simulation results without any parametrization of the algorithm, which makes it a useful method for the preliminary study of active colloids, prior to experimental work.

## 1 Introduction

Nano- to micro-meter scaled self-moving colloids have become a commonplace experimental device in soft-matter research groups, using a variety of driving methods including catalytic chemical reactions [1, 2] or laser illumination [3, 4]. The interest for these self-propelled particles, hereafter termed generically nanomotors as in Ref. [5], stems both from their envisioned applications in nanotechnology [5–7] and from the fundamental scientific insights offered by such devices [1, 8, 9]. Given their small sizes, typical of colloidal systems, the trajectories of nanomotors combine self-propulsion with the thermal fluctuations that are the signature of Brownian motion. Non-spherical colloids provide, even in the absence of self-propulsion, a nontrivial realisation of Brownian motion with a possibly non-diagonal diffusion matrix that couples the translational and rotational degrees of freedom [10, 11]. The detailed experimental study of Brownian dynamics for model anisotropic colloids is relatively recent. The colloids have been realised either by photolithography [12] or by assembling spherical components [13]. The combination of self-propulsion and anisotropic colloids results in qualitatively new types of trajectories: circling patterns for Janus doublets [14] and L-shaped particles [3], and gravitaxis for L-shaped particles [15]. The self-assembly of active rods, acting as building blocks for supra-colloidal anisotropic active particles displays a similar phenomenology [16].

In order to assess the role played by the shape of a nanomotor, one can resort to numerical simulations to avoid costly trial and

error in experiments. Brownian dynamics simulation methods require the *a priori* knowledge of the mobility tensor (or resistance matrix) of a particle and cannot serve, by themselves, for the study of the shape. It is possible to compute directly the resistance matrix using Stokes equation, for instance using finite element methods [17]. Here, we use instead coarse grained hydrodynamic simulations to resolve directly the dynamics of complex-shaped colloids and of the self-generated flows. Our choice extends naturally to other situations, such as many-motor dynamics in which the resistance matrix also depends on the distance and relative orientation to other motors, and integrates well with the mesoscopic chemical kinetics.

In this article, we study the L-shaped active colloid (or L motor, for short), explored experimentally by Kümmel *et al* [3], using Molecular Dynamics simulations. We describe in section 2 the mesoscopic simulation method [18, 19], in which the dynamics of both the colloid and the surrounding fluid particles is resolved. We present the bead model for the L shaped colloid in section 3. In section 4, we perform simulations of the equilibrium Brownian dynamics of the L particle and identify the center of hydrodynamics for the colloid in the quasi-2D geometry from the numerical data. Second, we perform simulations of the L motor when the chemical activity induces self-propulsion. We observe circling trajectories that result from the combined translational force and the torque applied by the self-propelling force. Third, we demonstrate the role played by self-generated hydrodynamic flows by considering an alternative dynamical model for the fluid particles' dynamics, in which the conservation of energy and momentum do not hold and no circling is observed. Finally, we discuss our results in section 5 and cast them in the perspective of active matter research.

## 2 Mesoscopic simulation method

We consider a system with a single L-shaped colloid and a fluid of point particles. The colloid consists in a rigid assembly of spherical beads of species  $C$  or  $N$ . The catalytic  $C$  beads activate the conversion of fuel into product and the non-catalytic  $N$  beads are chemically inert. The fluid consists of a large number of point particles of species  $A$  and  $B$ , of mass  $m$  for both species, with a number density per unit volume  $\gamma$  and a mass density  $\rho = \gamma m$ .

The colloid and the solvent in its vicinity evolve according to Molecular Dynamics, using the velocity Verlet algorithm [20, 21]. To integrate the equations of motion for the colloid constructed as a bead assembly, we use the quaternion-based velocity Verlet integrator described in Ref. [22]. The dynamics of the solvent, in all regions where it is force-free, is given by the coarse grained Multiparticle Collision Dynamics (MPCD) algorithm [23]. The fluid is partitioned every time interval  $\tau$  in a lattice of cubic cells of side  $a$  in which the velocities are exchanged according to an energy and momentum conserving rule. We use the truncated Lennard-Jones potential to couple the colloids and the solvent

\*ORCID:0000-0002-6640-6463

particles:

$$V_{\kappa,\alpha}(r) = 4\epsilon_{\kappa,\alpha} \left( \left( \frac{\sigma}{r} \right)^{12} - \left( \frac{\sigma}{r} \right)^6 + \frac{1}{4} \right) \quad (1)$$

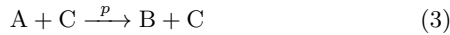
for  $r \leq \sigma \times 2^{1/6}$ .  $\kappa$  denotes the colloid species, which can be either ‘‘C’’ for catalytic colloids or ‘‘N’’ for noncatalytic colloids, and  $\alpha$  the solvent species. In the present work, we keep the scale parameter  $\sigma$  equal for all species pairs and set  $\epsilon_{\kappa,\sigma}$  to non-equal values to obtain different relative repulsion strengths at the surface of the colloid. We use a quasi-2D geometry as the corresponding experiment was confined between two glass plates. The coordinates  $x$  and  $y$  are periodic and the coordinate  $z$  is bounded by walls at  $z = 0$  and  $z = L_z$ . For the fluid particles, the walls in the  $z$  direction perform bounce-back collisions [24, 25] and include ghost particles during the collision step [26]. For the colloid, we apply a confinement potential in the  $z$  direction as

$$V(z) = \epsilon_w \left\{ \frac{3\sqrt{3}}{2} \left( \left( \frac{\sigma_w}{z - z_w^*} \right)^9 - \left( \frac{\sigma_w}{z - z_w^*} \right)^3 \right) + 1 \right\}, \quad (2)$$

where  $\epsilon_w$  is the strength of the potential,  $\sigma_w$  its scale and  $z_w^*$  is a shift of the potential’s origin.

We use the units system consistently defined by  $m = 1$  for the mass,  $\epsilon_{N,A} = \epsilon_{C,A} = 1$  for the energy and  $a = 1$  for the length. The unit of time is  $a\sqrt{m/\epsilon}$ .

To achieve a chemical reaction that is localised on the active part of the colloid, the beads of species ‘‘C’’ trigger the chemical reaction



in the fluid [19]. The reaction is carried out with probability  $p$  when the triggered solvent particle exits of the interaction range of the colloid to avoid discontinuities in the trajectory. We keep the simulation out of chemical equilibrium with a bulk reaction, using the reactive MPCD (RMPCD) algorithm [9, 27]



The bulk reaction is carried cell-wise and, similarly to what is done for the catalytic reaction (3), cells for which one or more fluid particles are interacting with colloids are excluded from the reaction process.

We list the simulation parameters for the fluid in table 1, along with the theoretical values for the transport coefficients of the fluid.

Parameter	Value
$k_B T$	1
$\rho$	10
$\tau$	0.1
$\gamma$	10
MPCD collision angle	$\pi/2$
Transport coefficients	
Viscosity $\eta$	5.43
$D_{\text{fluid}}$	0.117
Sc	4.7

Table 1: Simulation parameters for the fluid. The viscosity and self-diffusion coefficients are computed using formulas (52) and (43) of Ref. [28].

In order to assess the role of hydrodynamics, we also perform simulations in which we replace the MPCD collision step by a

random sampling (RS) [29] of the fluid particles’ velocities. At fixed time intervals  $\tau$ , instead of colliding the particles cell-wise, we draw their velocities from a thermal distribution. With the RS method, we still follow the fluid particles’ positions as they are necessary to generate chemical concentration gradients in the system. Using this alternative dynamical evolution for the fluid, we cannot match the dynamical properties of the colloid to the ones of the MPCD simulation [30]. Instead, we use it to compare qualitatively the colloid’s dynamics with and without hydrodynamics.

We perform all simulations with the open-source package RMPCDMD [18, 31, 32] and provide all the parameter and analysis files in appendix A and in the supplementary information [33].

### 3 Bead model for the L particle

The simulation strategy outlined in section 2 was first demonstrated for dimer nanomotors [19], in which only two beads make up the colloid. It has also been used since for bead models, such as for the Janus particle [34]. Chemically induced self-propulsion is well studied in simulations and has been analysed in great detail [35, 36], which makes it useful as a reference.

Here, we design a L particle whose foot is catalytically coated, following the geometry of Ref. [3]. In this latter work, however, the propulsion arises from the laser heating-induced demixion of the solvent at the Au-coated side of the colloid, a self-propulsion mechanism pioneered in Volpe *et al* [4]. In demixion-based propulsion, the local phase change in the fluid produces hydrodynamic flows whose reciprocal effect enable the motion of the colloid. Despite the difference in the type of motor, the hydrodynamic features of the present self-diffusiophoretic mechanism fall in the same category of phoretic motion [37]. In both situations, the motor and the surrounding fluid are force-free and it is the generation of flows that is responsible for self-propulsion.

We assemble beads in a L-shaped colloid, formed by an array of equally spaced beads and represented in Fig. 1. The figure shows the particle with its principal axes aligned with the laboratory frame coordinates (the x-y coordinates of the figure). As in Ref. [3], we also define a coordinate system aligned with the arms of the L. We illustrate those coordinates in Fig. 1.

## 4 Results

Parameter	Value
$L_x, L_y, L_z$	50, 50, 13
Number of solvent particles	325000
Number of beads	108
MD time step	0.01
Simulation length	$10^6 \tau$
Lennard-Jones $\sigma$	1.5
$\epsilon_{\kappa B}$	5
$k_2$	0.01
$\epsilon_w$	1
$\sigma_w$	1.5
$z_w^*$	3.5
Number of equilibrium simulations	20
Number of self-propelled simulations	20

Table 2: Simulation parameters for the L particles. See table 1 for the parameters of the MPCD fluid.

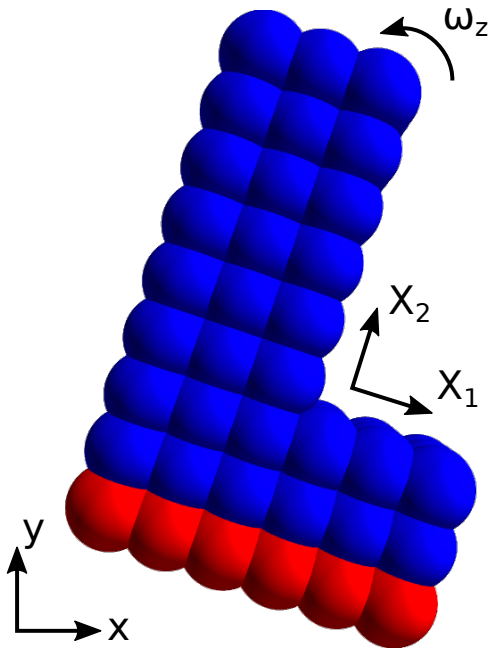


Figure 1: The bead assembly for the L-shaped colloid.  $x$  and  $y$  denote the lab-frame coordinates, coinciding with the principal axes of the body for  $t = 0$ .  $X_1$  and  $X_2$  denote the unit vectors along the short and long arm of the L, respectively, and  $\omega_z$  is the in-plane rotational velocity. We identify the third coordinate as the total angular displacement in the  $x$ - $y$  plane:  $X_3(t) \equiv \theta(t) = \int_0^t dt' \omega_z(t')$ . There are three layers in the  $z$  direction, totalling 108 beads.

#### 4.1 Brownian dynamics of the L particle

We perform equilibrium simulations of the L particle by setting the reaction probability  $p = 0$ . We list all simulation parameters in tables 1 and 2.

Prior to showing the simulation results for the diffusion of the L particle, we introduce an overdamped Langevin dynamical model for Brownian motion in two dimensions. The model is equivalent to the one found in Ref. [3] but we have chosen to write it in the body-frame coordinates so that we can write the diffusion as a constant matrix, following Ref. [38]. The evolution of the positions is given by

$$\begin{pmatrix} \dot{X}_1 \\ \dot{X}_2 \\ \dot{X}_3 \end{pmatrix} = \sqrt{2D^L} \zeta + \beta D^L F, \quad (5)$$

where  $X_1$  and  $X_2$  are the coordinates shown in Fig. 1,  $X_3$  is the angle of the particle in the  $x$ - $y$  plane,  $D^L$  is the diffusion matrix,  $\zeta$  is a vector white noise process and  $F$  is an external force that models, when non-zero, the effect of self-propulsion [3, 39]. We will use the model in Eq. (5) for three purposes: define the measurements of the diffusion matrix  $D^L$ , locate the center of hydrodynamics of the colloid, and estimate the radius of the circles in the self-propelled regime. We use the cross-displacement  $C_{ij}(\tau)$ , as defined in Ref. [13]:

$$C_{ij}(\tau) = \langle (X_i(\tau) - X_i(0))(X_j(\tau) - X_j(0)) \rangle. \quad (6)$$

The diagonal elements of  $C_{ij}(\tau)$  are the usual mean-squared displacements that represent diffusion. The coupling between

the degrees of freedom results in non-zero *off-diagonal* elements in  $C_{ij}(\tau)$ . From a fit of the linear-in-time evolution of the cross-displacement, we identify the diffusion matrix

$$C_{ij}(\tau) \propto 2D_{ij}^L \tau \quad (7)$$

that quantifies the dynamics of the L particle [12, 13, 38].

We show in Fig. 2 (full lines) the average cross-displacements of the L particle in equilibrium, where we use the center of mass (CoM) as the tracking point of the colloid. We obtain the following diffusion matrix by linear fits of the cross-displacement data:

$$D^{L@CoM} = \begin{pmatrix} 12.04 & -1.05 & 0.30 \\ -1.05 & 14.93 & -0.24 \\ 0.30 & -0.24 & 0.49 \end{pmatrix} \times 10^{-4}. \quad (8)$$

All degrees of freedom appear to be coupled. Apart for screw-type shapes, it is possible to identify the Center of Hydrodynamics of the colloid, where the coupling between translation and rotation disappears. Chakrabarty *et al* [38] provide a method to find the CoH for 2D Brownian colloids, which we apply here. The relevant locations on the colloid are the center of mass (CoM), whose trajectory is resolved in the simulation, and the center of hydrodynamics (CoH). Both locations are shown in Fig. 3. By definition, at the CoH the coupling between translation and rotation is zero in two dimensional systems [38, 40]. For two-dimensional Brownian motion, Chakrabarty *et al* [38] have used an overdamped Langevin model to compute the diffusion matrix at points other than the CoH (such as the experimental tracking point) and also the shift necessary to locate the CoH. In the reference frame of Fig. 1, the relation between the two points is given by

$$\begin{cases} X_{1,CoH} &= X_{1,CoM} + d_1 \\ X_{2,CoH} &= X_{2,CoM} + d_2 \end{cases}, \quad (9)$$

where  $d_1 = -D_{2,\theta}^L/D_{\theta}^L$  and  $d_2 = D_{1,\theta}^L/D_{\theta}^L$ .

We show in Fig. 2 (dashed lines) the cross-displacements of the L particle, using the center of hydrodynamics (CoH) as the tracking point. In comparison to the CoM results, the angular displacement is now uncorrelated to the translational displacements. Fitting the results of Fig. 2, we obtain the diffusion matrix  $D^{L,CoH}$  at the CoH:

$$D^{L@CoH} = \begin{pmatrix} 11.86 & -0.90 & -0.00 \\ -0.90 & 14.81 & 0.00 \\ -0.00 & 0.00 & 0.49 \end{pmatrix} \times 10^{-4}. \quad (10)$$

To obtain the forces and torque exerted on the L particle by a self-propelling force  $F = (0, F, l F)$ , we need the lever length  $l$  given by the distance between the center of the catalytically coated foot of the colloid and the CoH. Considering the location of the CoH ( $X_{1,CoM} + d_1, X_{2,CoM} + d_2$ ), the distance along axis  $X_1$  to the center of the foot of the L, where the force is applied, is  $l = 0.638$ . The CoH remains to the left of the colloid, in comparison to the center of the foot. We thus expect the torque to generate anticlockwise rotation.

#### 4.2 Self-propulsion of the L-shaped particle

By enabling the catalytic reaction (3) (i.e. setting the reaction probability to  $p = 1$ ), the fuel is converted on the active part of the L particle. We show the concentration field  $c_B$  of the B solvent species in Fig. 4 and the velocity profile of the fluid in Fig. 5.  $c_B$  is maximal close to the catalytic surface of the L and decreases rapidly due to the bulk reaction (4).

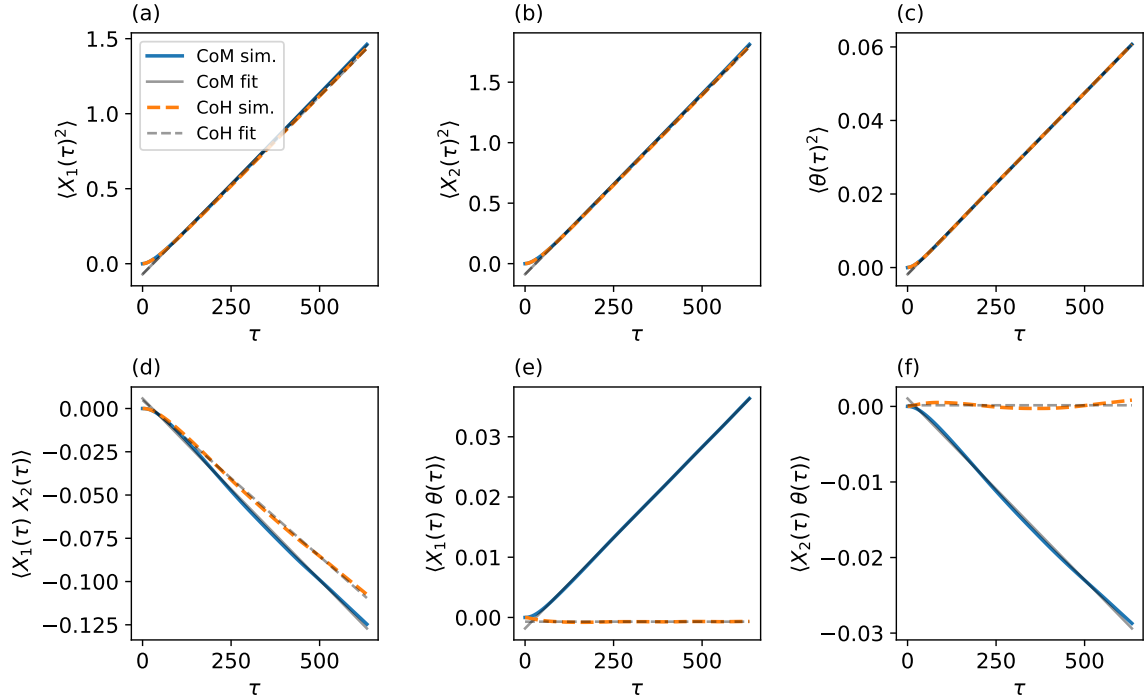


Figure 2: The cross-displacements  $C_{ij}(\tau)$  [Eq. (6)] for the L particle in equilibrium. The thick lines show the simulation data when tracking the CoM (full line) and the CoH (dashed line). The shaded lines are the corresponding linear fits. When tracking the CoH, the translation-rotation coupling disappears [panels (e) and (f)].

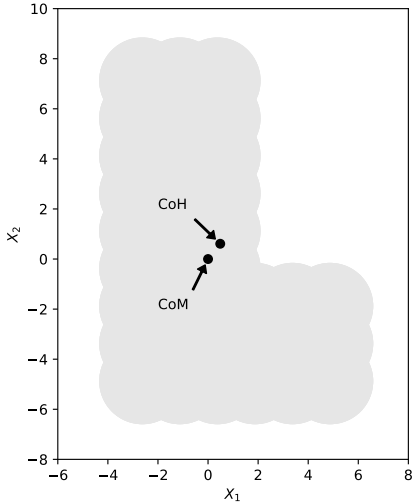


Figure 3: Flat representation of the bead model with the center of mass (CoM) and the center of hydrodynamics (CoH).

The L-particles, under nonequilibrium condition, display a self-propelling behaviour in combination with thermal fluctuations. We show example trajectories in Fig. 6, in which we notice that the motion features a curved path. This is at variance with the Brownian motion of isotropic particles.

We highlight the systematic character of the rotation in Fig. 6

by displaying six of the trajectories for the self-propelled L particle. Across all simulations, we compute the radius of the trajectories as the ratio of the translational velocity to the angular velocity  $\omega_y$  [3]. The mean radius is  $R \approx 55 \pm 7$ , with the error taken as the standard deviation over the 20 simulations. We compare this value to the average velocity resulting from a constant force

$$F_{\text{cst}} = \begin{pmatrix} 0 \\ F \\ -l_L F \end{pmatrix} \quad (11)$$

on the motor in Eq. (5). The presence of the third element in  $F_{\text{cst}}$  originates in the torque due to the misalignment of the applied force on the foot of the L with the center of hydrodynamics of the particle [3], with a lever length  $l$ . The average velocities are given by

$$\begin{pmatrix} \dot{X}_1 \\ \dot{X}_2 \\ \dot{X}_3 \end{pmatrix} = \beta F D^{L@CoH} F_{\text{cst}} \quad (12)$$

and the radius is

$$R = \frac{\sqrt{\dot{X}_1^2 + \dot{X}_2^2}}{\dot{X}_3} \approx 47 \quad (13)$$

for a lever length  $l = 0.638$  (see section 4.1). The diffusion matrix  $D^{L@CoH}$  and the position of the CoH thus provide a reasonable estimate of the rotation radius of the L nanomotor. The overdamped Langevin model does not capture the hydrodynamic tails, which may limit its accuracy.

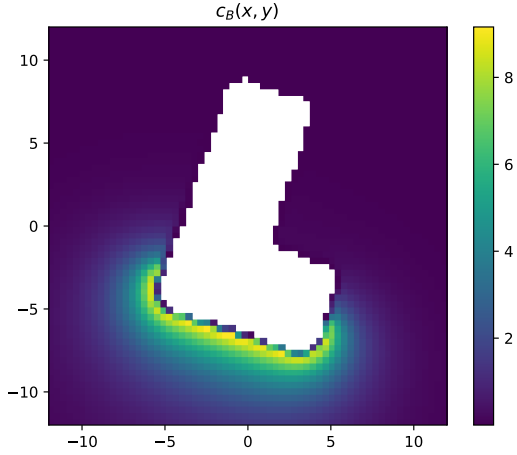


Figure 4: The concentration of solvent species B around the L particle for a single self-propelled simulation, averaged over time. The solvent particles are sampled in the mid-plane of the L particles in a layer of thickness 1. The blank region is the inner volume of the colloid.

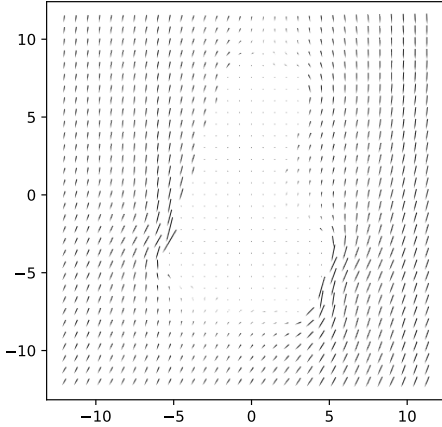


Figure 5: Velocity field of the fluid around the L particle for a single self-propelled simulation, averaged over time. The sampling is performed relative to the colloid's center of mass velocity.

### 4.3 The role of hydrodynamics in self-propulsion

We present here simulations of the L nanomotor in which the fluid particles' dynamical evolution follows the random sampling (RS) method. We use equal parameters for the number density  $\gamma = 10$ , the temperature  $k_B T = 1$  and for the solvent-colloid interaction and the wall-colloid interaction (see table 2). We resample the fluid's velocities every interval  $\tau = 2$ .

The simulations in Fig. 7 show that the motors move in spite of the fluid not resolving hydrodynamic flows. There is actually another possible self-propulsion mechanism that occurs when a concentration gradient is combined with non-equal surface interaction, as it is the case here. This density-gradient induced self-propulsion, already investigated in Ref. [19], usually contributes in addition to self-diffusiophoresis but it is here the only source of active motion.

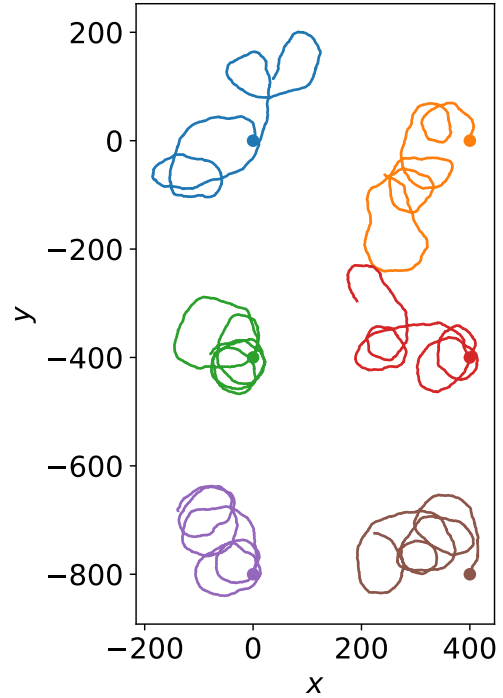


Figure 6: Six example trajectories for the self-propelled L particle from independent simulations. The large dot for each trajectory indicates the starting point. The trajectories are shifted for display purposes. Circling trajectories appear for all simulation runs and are combined with thermal fluctuations.

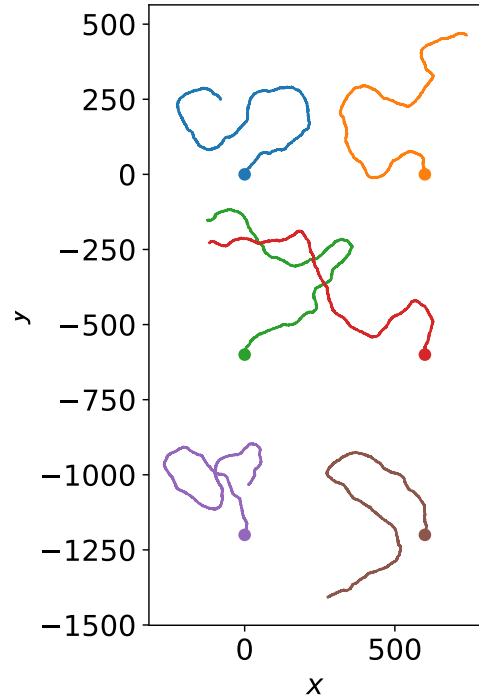


Figure 7: Same as Fig. 6 when hydrodynamics is turned off (RS fluid). There is no systematic orientation, at variance with the hydrodynamic (MPCD) simulations.

In the RS simulations, however, the friction arises from randomly moving solvent particles that act as a rather expensive thermostat. There is in consequence no center of hydrodynamics at which the hydrodynamic friction would apply and, in conjunction with the opposite self-propelled force, cause a torque on the colloid. The trajectories in Fig. 7 do not show any sign of circling behaviour, highlighting that, even for single-particle studies, hydrodynamically resolved fluids play an important role in simulation models.

## 5 Conclusions

Chemically powered nanomotors represent promising devices to autonomously execute tasks at the nano- and micro-scale [6, 7, 41–44]. Among the many challenges to resolve is the control of individual nanomotor trajectories as a function of their shape and functionalization. It is thus beneficial for the chemical, physical and engineering communities to improve the abilities of our computational modeling toolkit. Mesoscopic simulations have demonstrated their usefulness for understanding the mechanisms of chemical [5, 19, 34, 35, 45, 46] and thermal self-propulsion [34, 47].

Building on the work of Rückner and Kapral [19] and on rigid-body Molecular Dynamics [22], we extended the applicability of coarse-grained nanomotor simulations to the L particle. Considering first passive Brownian motion, we showed the coupling between the degrees of freedom, when tracking the center of mass of the colloid. By locating the center of hydrodynamics [38], we were able to decouple the rotational degrees of freedom from the translational ones and to obtain the actual lever length for the self-propulsion induced torque. In the active motion of the L particle, we find the same circling type of trajectories as in Ref. [3].

In the present work, the mobility matrix of the particles emerges from the colloid–fluid interaction, so that the circling patterns results directly from the shape of the particle without further input to the simulation procedure. To our knowledge, those are the first such simulation results for the symmetry class “asymmetric boomerang”, following the naming scheme of Chakrabarty *et al* [38]. As such, our results directly support the use anisotropic colloids for the study of (i) many-motor systems [30], (ii) the inclusion of external fields (flows and/or chemical gradients) [48], or (iii) sedimentation [15, 49], either in support or in preparation of experiments.

## Acknowledgements

Pierre de Buyl is a postdoctoral fellow of the Research Foundation-Flanders (FWO). The author wishes to thank Enrico Carlon, Peter Colberg, Thibaut Demaerel, Carlos Echeverria, Pavlik Lettinga, Stefanos Nomidids, and Snigdha Thakur for many discussions, and Christian Maes for support. The author is grateful to Raymond Kapral for initiating this line of research, for many interesting discussions, and for comments on the manuscript.

## A Computational reproducibility

We describe here the practical computational details to reproduce the present work.

We ran all the simulations with the program `single_body` from the open-source package RMPCDMD for the simulation of passive and chemically active colloids [18]. RMPCDMD is imple-

mented in Fortran 2008 and uses OpenMP for multithreaded operation. RMPCDMD outputs the trajectories in H5MD [50] files, a HDF5-based specification for molecular simulation data.

For the analysis, we used the Python programming language with the following libraries: NumPy [51] for the basic numerical layer, SciPy [52] for numerical integration, matplotlib [53] and Mayavi [54] for the figures, h5py [55] to read HDF5 files. We computed the mean-square displacements and cross-displacements with the package tidynamics [56]. We wrote the analysis of the simulation data in Jupyter notebooks<sup>1</sup> to the level that all the figures can be reproduced.

We uploaded the parameter and coordinate files and the notebooks for the analysis and figures to the Zenodo archival platform [33].

## References

- [1] Jonathan R Howse, Richard A. L Jones, Anthony J Ryan, Tim Gough, Reza Vafabakhsh, and Ramin Golestanian. Self-motile colloidal particles: From directed propulsion to random walk. *Phys. Rev. Lett.*, 99:048102, Jul 2007. doi:10.1103/PhysRevLett.99.048102.
- [2] Hua Ke, Shengrong Ye, R Lloyd Carroll, and Kenneth Showalter. Motion analysis of self-propelled pt-silica particles in hydrogen peroxide solutions. *J. Phys. Chem. A*, 114:5462–5467, 2010. doi:10.1021/jp101193u.
- [3] Felix Kümmel, Borge ten Hagen, Raphael Wittkowski, Ivo Buttinoni, Ralf Eichhorn, Giovanni Volpe, Hartmut Löwen, and Clemens Bechinger. Circular motion of asymmetric self-propelling particles. *Phys. Rev. Lett.*, 110:198302, May 2013. doi:10.1103/PhysRevLett.110.198302.
- [4] Giovanni Volpe, Ivo Buttinoni, Dominik Vogt, Hans-Jurgen Kummerer, and Clemens Bechinger. Microswimmers in patterned environments. *Soft Matter*, 7:8810–8815, 2011. doi:10.1039/C1SM05960B.
- [5] Raymond Kapral. Perspective: Nanomotors without moving parts that propel themselves in solution. *J. Chem. Phys.*, 138(2):020901, 2013. doi:10.1063/1.4773981.
- [6] S.J. Ebbens. Active colloids: Progress and challenges towards realising autonomous applications. *Cur. Opinion Coll. Interf. Sci.*, 21:14–23, 2016. doi:10.1016/j.cocis.2015.10.003.
- [7] Joseph Wang. *Nanomachines*. Wiley-VCH, Weinheim, Germany, 2013.
- [8] Jérémie Palacci, Cécile Cottin-Bizonne, Christophe Ybert, and Lydéric Bocquet. Sedimentation and effective temperature of active colloidal suspensions. *Phys. Rev. Lett.*, 105:088304, 2010. doi:10.1103/PhysRevLett.105.088304.
- [9] Snigdha Thakur and Raymond Kapral. Dynamics of self-propelled nanomotors in chemically active media. *J. Chem. Phys.*, 135:024509, 2011. doi:10.1063/1.3607408.
- [10] Howard Brenner. Coupling between the translational and rotational brownian motions of rigid particles of arbitrary shape i. helicoidally isotropic particles. *J. Colloid Sci.*, 20(2):104 – 122, 1965. doi:10.1016/0095-8522(65)90002-4.

<sup>1</sup><http://jupyter.org/>

- [11] Howard Brenner. Coupling between the translational and rotational brownian motions of rigid particles of arbitrary shape: II. general theory. *J. Colloid Interf. Sci.*, 23(3):407–436, 1967. doi:10.1016/0021-9797(67)90185-3.
- [12] Ayan Chakrabarty, Andrew Konya, Feng Wang, Jonathan V. Selinger, Kai Sun, and Qi-Huo Wei. Brownian motion of boomerang colloidal particles. *Phys. Rev. Lett.*, 111:160603, 2013. doi:10.1103/PhysRevLett.111.160603.
- [13] Daniela J. Kraft, Raphael Wittkowski, Borge ten Hagen, Kazem V. Edmond, David J. Pine, and Hartmut Löwen. Brownian motion and the hydrodynamic friction tensor for colloidal particles of complex shape. *Phys. Rev. E*, 88:050301, 2013. doi:10.1103/PhysRevE.88.050301.
- [14] Stephen J Ebbens, Richard A. L Jones, Anthony J Ryan, Ramin Golestanian, and Jonathan R Howse. Self-assembled autonomous runners and tumblers. *Phys. Rev. E*, 82:015304, Jul 2010. doi:10.1103/PhysRevE.82.015304.
- [15] Borge ten Hagen, Felix Kümmel, Raphael Wittkowski, Daisuke Takagi, Hartmut Löwen, and Clemens Bechinger. Gravitaxis of asymmetric self-propelled colloidal particles. *Nat. Commun.*, 5:4829, 2014. doi:10.1038/ncomms5829.
- [16] Megan S. Davies Wykes, Jeremie Palacci, Takuji Adachi, Leif Ristroph, Xiao Zhong, Michael D. Ward, Jun Zhang, and Michael J. Shelley. Dynamic self-assembly of microscale rotors and swimmers. *Soft Matter*, 12:4584–4589, 2016. doi:10.1039/C5SM03127C.
- [17] Johannes Voß and Raphael Wittkowski. Hydrodynamic resistance matrices of colloidal particles with various shapes. *arXiv*, page 1811.01269, 2018. <https://arxiv.org/abs/1811.01269>
- [18] Pierre de Buyl, Mu-Jie Huang, and Laurens Deprez. RMPCDMD: Simulations of colloids with coarse-grained hydrodynamics, chemical reactions and external fields. *J. Open Res. Softw.*, 5:3, 2017. doi:10.5334/jors.142.
- [19] Gunnar Rückner and Raymond Kapral. Chemically powered nanodimers. *Phys. Rev. Lett.*, 98:150603, Apr 2007. doi:10.1103/PhysRevLett.98.150603.
- [20] M. P. Allen and D. J. Tildesley. *Computer Simulation of Liquids*. Clarendon Press, Oxford, 1987.
- [21] Anatoly Malevanets and Raymond Kapral. Solute molecular dynamics in a mesoscale solvent. *J. Chem. Phys.*, 112:7260, Apr 2000. doi:10.1063/1.481289.
- [22] Dmitri Rozmanov and Peter G. Kusalik. Robust rotational-velocity-verlet integration methods. *Phys. Rev. E*, 81:056706, May 2010. doi:10.1103/PhysRevE.81.056706.
- [23] Anatoly Malevanets and Raymond Kapral. Mesoscopic model for solvent dynamics. *J. Chem. Phys.*, 110:8605, May 1999. doi:10.1063/1.478857.
- [24] E Allahyarov and G Gompper. Mesoscopic solvent simulations: Multiparticle-collision dynamics of three-dimensional flows. *Phys. Rev. E*, 66:036702, 2002. doi:10.1103/PhysRevE.66.036702.
- [25] Jonathan K Whitmer and Erik Luijten. Fluid–solid boundary conditions for multiparticle collision dynamics. *J. Phys. Condens. Matt.*, 22(10):104106, 2010. doi:10.1088/0953-8984/22/10/104106.
- [26] A Lamura, G Gompper, T Ihle, and D. M Kroll. Multiparticle collision dynamics: Flow around a circular and a square cylinder. *EPL (Europhysics Letters)*, 56:319, 2001. doi:10.1209/epl/i2001-00522-9.
- [27] Katrin Rohlf, Simon Fraser, and Raymond Kapral. Reactive multiparticle collision dynamics. *Comput. Phys. Commun.*, 179:132, 2008. doi:10.1016/j.cpc.2008.01.027.
- [28] Raymond Kapral. Multiparticle collision dynamics: simulation of complex systems on mesoscales. *Adv. Chem. Phys.*, 140:89, 2008. doi:10.1002/9780470371572.ch2.
- [29] M. Belushkin, R. G. Winkler, and G. Foffi. Role of fluid-density correlations in hydrodynamics: a multiparticle collision dynamics simulation study. *Soft Matter*, 8:9886–9891, 2012. doi:10.1039/C2SM26107C.
- [30] Peter H. Colberg and Raymond Kapral. Many-body dynamics of chemically propelled nanomotors. *J. Chem. Phys.*, 147(6):064910, 2017. doi:10.1063/1.4997572.
- [31] Pierre de Buyl, Peter H. Colberg, Laurens Deprez, and Mu-Jie Huang. RMPCDMD, 2016. URL <https://doi.org/10.5281/zenodo.198599>. Software release 1.0.
- [32] Pierre de Buyl, Peter H. Colberg, Laurens Deprez, and Mu-Jie Huang. RMPCDMD, 2015-2018. <http://lab.pdebuy1.be/rmpcdmd/>.
- [33] Pierre de Buyl. Complex nanomotors, 2018. URL <https://doi.org/10.5281/zenodo.1169907>. <https://doi.org/10.5281/zenodo.1169907>.
- [34] P. de Buyl and R. Kapral. Phoretic self-propulsion: a mesoscopic description of reaction dynamics that powers motion. *Nanoscale*, 5:1337–1344, January 2013. doi:10.1039/c2nr33711h.
- [35] Shang Yik Reigh and Raymond Kapral. Catalytic dimer nanomotors: continuum theory and microscopic dynamics. *Soft Matter*, 11:3149–3158, 2015. doi:10.1039/C4SM02857K.
- [36] Shang Yik Reigh, Mu-Jie Huang, Jeremy Schofield, and Raymond Kapral. Microscopic and continuum descriptions of janus motor fluid flow fields. *Phil. Trans. R. Soc. A*, 374(2080), 2016. doi:10.1098/rsta.2016.0140.
- [37] John F. Brady. Particle motion driven by solute gradients with application to autonomous motion: continuum and colloidal perspectives. *J. Fluid Mech.*, 667:216–259, 2011. doi:10.1017/S0022112010004404.
- [38] Ayan Chakrabarty, Andrew Konya, Feng Wang, Jonathan V. Selinger, Kai Sun, and Qi-Huo Wei. Brownian motion of arbitrarily shaped particles in two dimensions. *Langmuir*, 30(46):13844–13853, 2014. doi:10.1021/la5037053.

- [39] Borge ten Hagen, Raphael Wittkowski, Daisuke Takagi, Felix Kümmer, Clemens Bechinger, and Hartmut Löwen. Can the self-propulsion of anisotropic microswimmers be described by using forces and torques? *J. Phys.: Condens. Matter*, 27(19):194110, 2015. doi:10.1088/0953-8984/27/19/194110.
- [40] J. Happel and H. Brenner. *Low Reynolds number hydrodynamics - with special applications to particulate media*. Kluwer, Dordrecht, 1991.
- [41] Jaideep Katuri, Xing Ma, Morgan M. Stanton, and Samuel Sánchez. Designing micro- and nanoswimmers for specific applications. *Acc. Chem. Res.*, 50(1):2–11, 2017. doi:10.1021/acs.accounts.6b00386.
- [42] Berta Esteban-Fernández de Ávila, Mingjiao Zhao, Susana Campuzano, Francesco Ricci, José M. Pingarrón, Marcello Mascini, and Joseph Wang. Rapid micromotor-based naked-eye immunoassay. *Talanta*, 167:651 – 657, 2017. ISSN 0039-9140. doi:10.1016/j.talanta.2017.02.068.
- [43] L. Baraban, M. Tasinkevych, M. N. Popescu, S. Sanchez, S. Dietrich, and O. G. Schmidt. Transport of cargo by catalytic janus micro-motors. *Soft Matter*, 8:48–52, 2012. doi:10.1039/C1SM06512B.
- [44] A. Aubret, S. Ramananarivo, and J. Palacci. Eppure si muove, and yet it moves: Patchy (phoretic) swimmers. *Cur. Opinion Coll. Interf. Sci.*, 30:81 – 89, 2017. doi:10.1016/j.cocis.2017.05.007.
- [45] Mingcheng Yang, Adam Wysocki, and Marisol Ripoll. Hydrodynamic simulations of self-phoretic microswimmers. *Soft Matter*, 10:6208–6218, 2014. doi:10.1039/C4SM00621F.
- [46] Leonardo F Valadares, Yu-Guo Tao, Nicole S Zacharia, Vladimir Kitaev, Fernando Galembeck, Raymond Kapral, and Geoffrey A Ozin. Catalytic nanomotors: Self-propelled sphere dimers. *Small*, 6:565–572, Feb 2010. doi:10.1002/sml.200901976.
- [47] Mingcheng Yang and Marisol Ripoll. Simulations of thermophoretic nanoswimmers. *Phys. Rev. E*, 84:061401, 2011. doi:10.1103/PhysRevE.84.061401.
- [48] Laurens Deprez and Pierre de Buyl. Passive and active colloidal chemotaxis in a microfluidic channel: mesoscopic and stochastic models. *Soft Matter*, 13:3532–3543, 2017. doi:10.1039/C7SM00123A.
- [49] Jan-Timm Kuhr, Johannes Blaschke, Felix Rühle, and Holger Stark. Collective sedimentation of squirmers under gravity. *Soft Matter*, 13:7548–7555, 2017. doi:10.1039/C7SM01180F.
- [50] Pierre de Buyl, Peter H. Colberg, and Felix Höfling. H5MD: A structured, efficient, and portable file format for molecular data. *Comp. Phys. Commun.*, 185:1546–1553, 2014. doi:10.1016/j.cpc.2014.01.018.
- [51] Stefan van der Walt, Steven Chris Colbert, and Gaël Varoquaux. The numpy array: A structure for efficient numerical computation. *Comput. Sci. Eng.*, 13:22–30, 2011. doi:10.1109/MCSE.2011.37.
- [52] Eric Jones, Travis Oliphant, Pearu Peterson, et al. SciPy: Open source scientific tools for Python, 2001–. URL <http://www.scipy.org/>.
- [53] J. D. Hunter. Matplotlib: A 2d graphics environment. *Comput. Sci. Eng.*, 9(3):90–95, 2007. doi:10.1109/MCSE.2007.55.
- [54] Prabhu Ramachandran and Gaël Varoquaux. Mayavi: 3d visualization of scientific data. *Comput. Sci. Eng.*, 13(2):40–51, 2011. doi:10.1109/MCSE.2011.35.
- [55] Andrew Collette. *Python and HDF5*. O’Reilly, 2013.
- [56] Pierre de Buyl. tidynamics: A tiny package to compute the dynamics of stochastic and molecular simulations. *Journal of Open Source Software*, 3(28):877, 2018. doi:10.21105/joss.00877.